PCCP

Accepted Manuscript

ROYAL SOCIETY OF CHEMISTRY

www.rsc.org/pccp

* Corresponding author. Tel.: 0091-820-2925072; fax: 0091-820-2570062
Email: sajan.george@manipal.edu

Tailoring of optical properties of fluorescein using green synthesized gold nanoparticles

Jisha John[a], Lincy Thomas[a], Nibu A. George[b], Achamma Kurian[a] and Sajan D. George[c*]

[a] *Photonics lab, Department of physics, Catholicate college, Pathanamthitta, India– 689645*

[b] *Baselius College, Kottayam, India-686001*

[c] *Centre for atomic and molecular physics, Manipal university, Manipal, Karnataka, India – 576104*

Abstract

The dye-nanoparticle mixtures hold great promise in biological as well as photonics applications due to their capability to tailor the emission behavior of dye by tuning the nanoparticles parameters. However, as compared to well defined dye-nanoparticle distance, studies lack understanding of homogenous mixture of dye and nanoparticles. In this work, we investigate the influence of shape and concentration of gold nanoparticles prepared via green synthesis on the optical properties of fluorescein dye in a dye-nanoparticle mixture. We have investigated the radiative path of deexcitation using steady state fluorescence and non-radiative path is probed using laser based dual-beam thermal lens technique. The energy transfer efficiency as well as dye-nanoparticle distance is studied using both techniques. Further, we have explored the influence of nanoparticles parameters on the fluorescence quantum yield of fluorescein using thermal lens technique. The studies indicate that spherical nanoparticles are efficient quenchers while star shaped nanoparticles can probe larger dye-NP distances. The tailoring of dye properties by tuning nanoparticle parameters can be utilized in diverse areas including bioimaging, solar cells, and sensors.

Introduction

Recent years have been witnessing considerable research efforts to understand the dye-metal nanoparticles (MNPs) hybrid systems due to their potential applications in bioimaging, sensors and solar cells [1-5]. Despite a plethora of literature existing about energy transfer studies between dye molecule and MNPs at a pre-defined distance, a few studies reported on mixtures wherein MNPs homogenously mixed in certain ratio with an organic dye dissolved in a suitable solvent [6]. This kind of simple dye-NP hybrid is a prerequisite for many of the industrial as well as technological applications and thus detailed study of such mixtures are of paramount interest. In contrast to the dipole-dipole mediated Forster resonance energy transfer (FRET) mechanism of energy transfer between a conventional donor and an acceptor (dye-dye mixtures), the dye-NP systems reported to follow Nanometal Surface Energy Transfer (NSET) model. In the latter case, MNPs considered as an infinite plane of dipoles and the interaction scales as $1/d^4$ (where d is the distance between the NP surface and dipole), as oppose to $1/R^6$ dependence in the case of FRET, where R is the center-to-center dipole distance [7-9]. This favorable scaling allows dye-NPs mixture as a better optical ruler around the dye molecule against dye-dye mixtures. It is reported that the former can probe ~ 22 nm while the latter is efficient only up to 10 nm [10-11]. However, depending on the value of d, MNPs found to either enhance or quench the luminescence of nearby dye molecules. Thus, an investigation of MNPs parameters such as shape and concentration on the value of d as well as the emission behavior or quantum yield of dye molecules are of immense importance, not only from application point of view but also from understanding the energy transfer mechanism.

Amongst the various MNPs reported in literature, gold nanoparticles (AuNPs) are the most favorite candidate owing to their surface plasmon resonance in the visible range of the electromagnetic spectrum, high chemical stability, low cytotoxicity, biocompatibility, ease of preparation and surface functionalization etc., [12-14]. Of late, due to the toxicity of chemical methods and energy consumption in the conventional physical methods of AuNPs preparation, green synthesis is being used as an alternative method for preparing AuNPs [15]. In the green synthesis route, AuNPs prepared either using biological species such as bacteria, fungi etc., or using the plant's extract [16-18]. While the biological species require special environment for the preparation of NPs, the latter do not require special

environmental conditions. In general, extract from plant act as reducing agent and this technique allows possibility of scaling up as compared to biological species. Further, this approach enables tailoring of shape and size of the prepared NPs by controlling the external parameters such as concentration, pH etc. Hitherto, apart from the routine characterization and anti-bacterial activity of green synthesized particles, little work has been reported on the interaction of the green synthesized NPs with dyes.

In the present study, we have prepared star and spherical AuNPs using the extract from different plants, piper nigrum and cinnamomum verum respectively as reducing agents. The prepared NPs having various concentrations are mixed with fluorescein dye and investigated the emission behavior, energy transfer efficiency, dye-NPs distance in the mixture as well as fluorescence quantum yield (FQY). This particular dye-NPs mixture is chosen for the present study due to wide applicability of fluorescein among medical community and good spectral overlap between the emission spectrum of fluorescein and the absorption spectrum of the MNPs. The impetus of this work lies in the tailoring of intrinsic properties of fluorescein by varying the NPs parameters and thereby controlling the energy transfer mechanism that has tremendous use in bio-analytical as well as solar cell applications. In particular, the focus of the work presented here lies (i) how the concentration of differently shaped AuNPs (star and spherical AuNPs of average size 20 nm) prepared via green synthesis influences the energy transfer efficiency and the dye-NPs distance (ii) how the shape and concentration of NP influences FQY of fluorescein dye in a dye-NPs mixture. The first question is addressed via steady state fluorescence and laser based dual beam thermal lens (TL) technique, and the latter technique is employed to answer the second question. Whilst the steady state fluorescence technique relies on the radiative path of deexcitation of excited dye molecules, the TL technique probes the non-radiative mode of deexcitation. The complementary nature of the techniques are utilized to cross validate the dye-NPs particle distance as well as the energy transfer efficiency in AuNPs-fluorescein mixture, for differently shaped particles having various concentrations. Furthermore, the potential of presently employed photothermal technique, TL technique, to evaluate the FQY of dye molecules without usage of a fluorophore of known FQY is exploited to investigate the influence of AuNPs concentration as well as the shape of NP on FQY of fluorescein dye [19-20]. To the best of our knowledge, there is no report on the shape and concentration dependent energy transfer studies between green synthesized AuNPs and fluorescein dye in a mixture.

Experimental Section

1. Green synthesis of AuNPs

In the present study, the AuNPs are prepared by plant's extract as reducing agent instead of commonly used citrate in citrate reduction technique. The Gold (III) chloride trihydrate ($HAuCl_4 \cdot 3H_2O$, 99.99 %, Sigma-Aldrich) is taken as precursor which is reduced using extract from the piper nigrum and cinnamomum verum. More specifically, the piper nigrum and cinnamomum verum initially cleaned by washing many times with water followed by drying using water adsorbing paper. We have taken 3g of piper nigrum or cinnamomum verum and crushed in a mortar, dispersed in 15 ml of double distilled water and boiled for 10 minutes at 70-80^{0}C. The plant extract is then filtered and stored at 4^{0}C. To the 7ml of this extract, 1 mM of gold chloride trihydrate solution is added to obtain Au nanofluids. The formation of AuNPs causes a visual change in color of the solution from light yellow to cherry red.

2. Characterization of Au NPs –TEM studies

The size and shape of the Au colloids were investigated with a JEOL JEM 2100 TEM instrument operated at an accelerating voltage of 200 kV (JEOL 2100, JEOL Ltd., Japan). The samples for transmission electron microscope (TEM) studies were prepared by drop casting the solutions on carbon-coated copper grids and then dried at room temperature. The images obtained for Au nanofluids using piper nigrum and cinnamomum verum as reducing agent are shown in figure 1(a) and 1(b). In the former case, the shape of the NPs are found to be star shaped whereas for the latter case the shape of NP is spherical, clearly indicating the influence or origin of reducing agent, piperine in piper nigrum and cinnamonaldehyde in cinnamomum verum, in the green synthesis approach. However, in both cases, the average particle size is around 20 nm. It has already been reported that the green synthesis route can yield differently shaped particles, depending upon their environment. In the present case, the pH of Au nanofluid prepared from piper nigrum is 4.34 whereas for cinnamomum, pH is 2.92. The change in dielectric environment as well as pH can lead to the observed difference in shape of the prepared AuNPs.

3. Absorption studies of AuNPs

In order to explore the influence of shape on the collective oscillations of the electrons in the conduction band of the AuNPs (surface plasmon resonance of AuNPs that originate extinction spectra), UV-Vis spectrum of the star shaped as well as spherical shaped particles of concentration 2.57 nM are taken using a commercially available UV-Vis spectrophotometer (Shimadzu UV-2401 PC) is shown in figure 2. From the figure 2, it is clear that though the plasmonic absorption peaks at nearby wavelength for spherical and star shaped AuNPs, the plasmonic half width is more for star shaped particles. The plasmonic half width of AuNPs is associated with dephasing of coherence electron oscillations. The more efficient electron-electron collision mediated decoherence results in the decoherence of electron oscillations and results in a wider plasmonic absorption spectrum for star shaped AuNPs in comparison to spherical AuNPs [21]. The surface plasmonic absorption of spherical particles maximizing around 525 nm whereas star shaped particles is around 529 nm. In general, the peak position of the surface plasmon absorption band is dependent on the size of the MNPs as well as the dielectric constant of the metals and the medium surrounding the particle. The change in dielectric environment of the particles that arise from the difference in reducing agent employed is causing a slight shift in the absorption peak. In addition, for the particles of size considered here (~ 20 nm), the SPR absorption curve is independent of particle size. In addition to the change in dielectric environment, the uneven spiky surface of the star shaped particles may also contribute to the observed small red shift in the SPR peak. It has been reported in literature that the elongation or the tips of the NPs associated with red shift in the longitudinal surface plasmon peak [22-23]. However, the minimal shift in the present case clearly indicates that the aspect ratio of the particle is nearly same for spherical as well as star shaped NPs. It is pertain to note here that the UV-Vis absorption spectrum for Au nanofluids for all concentrations of differently shaped AuNPs investigated here also exhibit similar absorption spectral features (0.13, 0.51, and 1.79 nM, not shown here) and thereby implying the monodispersibility and the absence of NPs aggregation formation. The dye-NPs mixture is prepared by taking fluorescein dye (2.4×10^{-4} M) dissolved in ethanol and Au nanofluid of different concentrations in the ratio 1:2. The pH value of the fluorescein corresponding to the concentration employed here ~ 5. It is already reported that, based on the pH value, the molecules of fluorescein can exist in different prototropic isomeric form; neutral, cationic, anionic and dianionic. While the dye molecules exist in

cationic form in the highly acidic environment (pH<2), dianionic form is favored in highly alkaline environment (pH>8) [24]. However, for pH value between 3.3 and 5.5, the molecules exist in neutral as well as monoanionic isomeric forms. Thus, for the concentration considered here, the dye solution comprises of neutral and monoanionic isomers. More importantly, it has been reported that for the fluorescence emission profile of the dye molecules does not change much in highly alkaline (>8) and acidic (~ 1.5 to 5) environments [25]. A typical absorption spectrum of mixture comprising of fluorescein dye and nanofluid (0.51 nM) in the above mentioned ratio is shown in figure 3. From the figure, it is clear that mixture consists of dual peaks of fluorescein peaking around 450 nm and 470 nm with an addition peak arising from the surface plasmonic absorption of star and spherical AuNPs. It is already reported that the AuNPs of size ~ 20 nm have an extinction coefficient of the order of 10^9 M^{-1} cm^{-1} [26] which is much higher than that of fluorescein (2.9×10^4 M^{-1} cm^{-1}) [27]. Thus, the large extinction coefficient of AuNPs compared to dye molecules lead to the enhanced absorption values of the mixture [21]. The experimentally observed peaks of fluorescein are consistent with the earlier studies [27].

4. Thermal lens setup

In order to understand the influence of non-radiative energy transfer to the observed fluorescence quenching, all the samples are studied using TL technique that rely on non-radiative deexcitation of the sample. A schematic of the TL experimental setup used here is given in Supplementary information (Figure S1). In brief, the sample is excited with a mechanically chopped (Stanford Research Systems SR 540) Gaussian pump beam from a He-Cd laser operating at 442 nm (25mW). The non-radiative deexcitation of the sample causes localized temperature rise and due to negative temperature coefficient of refractive index, the sample now act like a diverging lens (TL) that mimic the profile of the pump beam [28-30]. A probe beam (He-Ne laser, 1mW) passing through so formed TL get diverged and can be collected at far using an optical fiber coupled with a photodetector. The output of the photodetector is measured using a lock-in amplifier for which the reference signal from the mechanical chopper is used. The transmitted pump beam to the detector is avoided by employing an appropriate filter and the pump and probe beam are made collinear by using a dichroic mirror. In the present study, the amplitude of TL signal is measured for all concentrations of AuNPs investigated here as well as for the corresponding dye-AuNPs mixtures.

Results and Discussions

1. Steady state fluorescence measurements

The fluorescence of fluorescein and fluorescein-AuNPs mixtures is measured using an experimental setup shown in supplementary information (figure S2). In this case, 442 nm from a He-Cd laser (25 mW) is used as source of excitation and fluorescence from the dye molecules mixed with star and spherically shaped AuNPs of various concentrations are recorded using a Monochormator-PMT assembly (PDS1, Dongwoo Optron Co. Ltd) with Monoworks software is given in figure 4 and 5. In both cases, the fluorescence of fluorescein that peaks around 512 nm quenches with an increase in NP concentration in the mixture. The photostability of the pristine dye measured by probing the steady state fluorescence for 100 minutes and shown in supplementary information (figure S3). It is clear that pristine dye is stable for much longer time scale compared to the experimental time scale of maximum 2 minutes. In the vicinity of MNPs, dyes are reported to either exhibit enhanced fluorescence or quenching behavior, depending upon the dye-NP distance. The modified emission arises as a consequence of non-radiative energy transfer to the MNP from the dye molecule, scattering and absorption by the MNPs, and changes in the emitter's radiative and non-radiative decay rates. Owing to the plasmonic field around, the NP can also lead to local field enhancement, particularly along equator plane that can result in an enhanced excitation rate, such a situation would lead to enhanced fluorescence of dye molecules in a dye-NP mixture. However, in all our cases, we observed quenching in the fluorescence of fluorescein dye which indicate that plasmonic field around the MNP interact with dye emission through other mechanisms. In fact, the relative orientation of the dye molecule and the MNP to the laser radiation determine whether the interaction contributes to the dye fluorescence enhancement or quenching. The relative orientation is a parameter that is difficult to control experimentally in a liquid mixture of dye and NP. In addition, dye-NP distance also plays crucial role in determining the influence of NP on the enhancement or quenching of dye fluorescence. For the AuNPs of sizes ~ 20 nm and concentration range employed here, the contribution from direct absorption and scattering of MNPs at 442 nm laser can be neglected. In general, the radiative decay time is determined by the extinction coefficient of the fluorophore and slightly dependent on the medium, thus it can be considered as a fixed parameter for dye-NP mixture considered here and emission characteristics as well as quantum efficiency is normally tailored by changing the non-radiative decay rate. It is

worthwhile to note here that for all dye-NP mixtures, the pH of the solution is between 3 and 5 wherein emission behavior of fluorescein is pH independent. Hence, the experimentally observed variation is not caused by the change in pH of the solution or the relative amount of various isomers in the mixture. The non-radiative energy transfer between the dye and MNP arise from the diffusive interaction lead to the dynamical quenching of the dye fluorescence. The static quenching that normally involve the complex formation of the fluorophore and the quenching in the ground state of the molecules can be neglected here as there is no indication of formation non-fluorescing product in the absorption spectrum of dye-NP mixture. The electron transfer mechanism mediated quenching of dye molecules in the vicinity of MNPs are dominant only when the size of MNP is < 5nm [31-32].

The dynamic quenching mediated by non-radiative energy transfer between the donor and acceptor molecules depend upon spectral overlap integral between the dye emission and the acceptor absorption. In general, the spectral overlap integral $J(\lambda)$ in the case of dye-NP interaction normally calculated from the expression $J(\lambda) = \int_0^\infty F_D(\lambda)\epsilon_A(\lambda)\,\lambda^4\,d\lambda\,M^{-1}cm^{-1}\,nm^4$, where λ is the wavelength in nm; $F_D(\lambda)$ represents the normalized fluorescence intensity at wavelength λ, $\epsilon_A(\lambda)$ is molar absorptivity of the acceptor at a given wavelength [33-34]. As is evident in figure (6), there is good spectral overlap between the emission spectrum of the dye molecules and the absorption spectrum of the AuNPs which suggest the possibility of efficient energy transfer between the fluorescein and AuNPs. However, the experimentally observed quenching in fluorescence implies that dye and NP are at a certain distance and the energy is efficiently transferred from the dye molecules to the MNPs.

2. Energy transfer studies

In situations wherein dynamic quenching is dominating, as in the present studies, Stern-Volmer equation provide a quantitative relation between luminescence intensity of donor in the absence and presence of an acceptor and is given by [35-36]

$$\frac{F_0}{F} = 1 + K_D[Q] \qquad (1)$$

where F_0 and F are the luminescence intensities in the absence and presence of acceptor, respectively, K_D is the Stern-Volmer quenching constant, Q is the acceptor concentration. In the case of quenching $F < F_0$, and the ration $\frac{F_0}{F}$ increases linearly with Q

while the fluorescence signal probes the radiative channel and thermal lens signal probe the corresponding non-radiative channel of deexcitation and it is based on the principle of energy conservation. Let P_L is the incident power beam and P_t is the transmitted power beam. The absorbed power is the sum of the laser power degraded to heat, P_{th}, and the luminescence emission, P_f, provided there occurs no photochemical reaction. Hence

$$\mathrm{P_L = P_{th} + P_f + P_t} \quad (2)$$

Corresponding to the quenching in fluorescence signal with concentration of acceptor, the TL signal strength increases with acceptor concentration, and hence $\eta_L^0 < \eta_L^A$ and the ratio η_L^0/η_L^A decreases with acceptor concentration, so that [37]

$$\frac{\eta_L^0}{\eta_L^A} = 1 - \mathrm{K_D[Q]} \quad (3)$$

Here η_L^0 and η_L^A are the TL signals without and with acceptor in the mixture. The fluorescence and TL ratio signal corresponding to the equation (1) and (3) for spherical as well as star AuNPs mixed fluorescein dye is shown in figure (7) and (8). For AuNPs of size 20 nm, $l = 1$, the dipolar mode is the predominant accepting mode of energy transfer.

The values of Stern-Volmer coefficient are estimated independently from steady state fluorescence and TL technique for star as well as spherical AuNPs dispersed dye-NP mixture. The values obtained from slope of the plots depicted as fluorescence signal ratio and TL signal ratio for spherical shaped particles is $0.213 \times 10^9 M^{-1}$ and $0.209 \times 10^9 M^{-1}$. Similarly the Stern-Volmer coefficient value obtained in the case of star shaped NPs are $0.150 \times 10^9 M^{-1}$ and $0.153 \times 10^9 M^{-1}$ respectively. In general, the enhancement in emission behavior of dye molecules due to the plasmonic field can be neglected for particle sizes greater than 10 nm [38-39]. The high value of the Stern-Volmer coefficient can be attributed to high molar extinction coefficient of 20 nm sized AuNPs and nanomolar binding affinity of organic dyes to gold nanoparticles. Moreover, in the preset case, there is good

spectral overlap between emission spectrum of the donor and the absorption spectrum of the acceptor. A high value of Stern-Volmer coefficient clearly indicates that very low concentration of AuNPs are sufficient to cause a substantial reduction in fluorescence intensity that is consistent with the experimental observation of NPs concentration dependent fluorescence quenching. Furthermore, the nearly equal values of the Stern-Volmer coefficient obtained from both techniques clearly exemplify the complementarily nature of the techniques.

Amongst the several models employed to explain the energy transfer between the MNP and dye molecule, NSET is reported to provide better correlation between the experiment and the theory. The NSET is based on the Persson-Lang surface energy model in which NP is considered as strongly coupled surface-localized dipoles that can approach a hemispherical approximation of a plane. According to this model, the distance at which dye displays equal probabilities for energy transfer and spontaneous emission is given by [40]

$$d_0 = \left(0.225 \frac{c^3 \phi_{dye}}{\omega_{dye}^2 \omega_F k_F} \right)^{1/4} \quad (4)$$

where ϕ_{dye} is the quantum efficiency of the dye, ω_{dye} is the frequency of the donor electronic transition, ω_F is the Fermi frequency, and k_F is Fermi wave vector of the metal. For the wavelength used here (442 nm) $\omega_{dye} = 4.26 \times 10^{15} s^{-1}$ and by using $\omega_F = 8.4 \times 10^{15} s^{-1}$, $\phi_{dye} = 0.79$, $k_F = 1.28 \times 10^8 cm^{-1}$, the value of d_0 is calculated as 71.40 Å. The experimental values for d_0 measured using Equation (7) are 70.795 Å and 72.02 Å respectively are in good agreement with the calculated value. Thus the distance dependent energy transfer efficiency from the fluorescein dye to AuNPs can be estimated from the steady state fluorescence signal strength using the equation [4]

$$\phi_{ET} = 1 - \frac{F}{F_0} \quad (5)$$

Considering the complementary nature of TL and fluorescence technique, the energy transfer efficiency can also be evaluated from the TL signal ratio using the equation [41]

$$\phi_{ET} = 1 - \frac{\eta_L^0}{\eta_L^A} \quad (6)$$

The value of energy transfer efficiency obtained for the different concentrations of the star as well as spherical AuNPs mixed with fluorescein are tabulated in table 1. From the table, it is clear that the values evaluated using both techniques agree well. A generic form that relates energy transfer efficiency to the distance between the dye and MNP, d is given [2]

$$\phi_{ET} = \frac{1}{1 + \left(\frac{d}{d_0}\right)^n} \quad (7)$$

Here $n = 6$ correspond to dipole-dipole transition mediated FRET and $n = 4$ corresponds to surface energy transfer (SET). Following the popular NSET, the dye-NP distance for differently shaped particles for all concentrations of NPs are evaluated and tabulated in table 1.

It is interesting to point out here that, despite the similar particle size and plasmonic absorption band, the energy transfer is more efficient in the case of spherical shaped AuNPs-fluorescein mixture as compared to star shaped AuNPs-fluorescein mixture. This is because the spherical symmetry of the NP creates a symmetrical plasmonic volume around the particle and energy transfer mechanism is dipole orientation dependent. However, in the latter case the angle between the dye dipole axis and NP dipole axis control the energy transfer [23, 42]. Moreover, at high quenching efficiency as in the present case, the experimental oscillator strength of dye molecules only contribute to 5-10 % of the decrease in intensity of fluorescence signal, not the experimentally observed 50-80%. This unambiguously in state that quenching occurs by means of NSET rather than change in radiative rate. Aside from the expected decrease in dye-NP distance with increase in NP concentration in the mixture, the distance between spherically shaped NP is found to smaller than star shaped NP for a given concentration. The NSET mechanism originates from the interaction of the electromagnetic field of the fluorophore dipole and the conduction electrons of the metals. In the case of MNPs, the electrons scatter predominantly to the surface of the

NP due to large curvature and the interaction is more efficient when the dipole orientation is perpendicular to the surface. However, as opposed to spherical AuNPs that create spherical plasmonic field around the NP, the star shaped NPs create anisotropic plasmonic field around the particle with increased strength around the tip [43-44]. Consequently, as evident here in the dye-NP distance measurements, star shaped NPs probe larger distances compared to the spherical NPs. The evaluated values of dye-NP distance are smaller than particle diameter so that SET model can be effectively utilized instead of FRET model.

3. Quantum Yield Measurements

The quantum yield of fluorescein dye molecules in the presence of star and spherical NPs of various concentrations is evaluated using the measured TL signal by following the theoretical approach outlined in the previous studies. In a completely fluorescence quenched sample, the entire excitation energy is converted into non-radiative relaxation process and hence, FQY, Q_f is given by [45-46]

$$Q_f = \frac{P_f}{AP_L}\frac{\lambda_f}{\lambda} = \left(1 - \frac{P_{th}}{P_\alpha}\right)\frac{\lambda_f}{\lambda} \tag{8}$$

where $P_\alpha = AP_L$. Here A is the absorbance of the material. The ratio of peak fluorescence wavelength λ_f to the excitation wavelength λ takes into account of the Stoke's shift. Here P_{th} is directly proportional to the thermal lens signal η and P_α is proportional to the thermal lens signal η_α corresponding to the concentration at which the fluorescence intensity quenches completely. Thus, in terms of thermal lens signal, the quantum yield can be written as

$$Q_f = \left(1 - \frac{\eta}{\eta_\alpha}\right)\frac{\lambda_f}{\lambda} \tag{9}$$

The measured values of FQY are shown in figure 9. The FQY decreases with an increase in NP concentration and the effect is more efficient in the case of spherical NPs compared to star shaped NPs. As mentioned previously, in the case of spherical NPs, the energy transfer phenomena is orientation independent whereas for the star shaped NPs, the plasmonic field around the particle is maximum around the edges and the energy transfer is orientation dependent. In the case of spherical NPs, the molecular dipoles are aligned parallel to NP dipole causing an efficient

quenching and reduction in FQY. However, for a star shaped particle of same size, the probability of dipoles aligning in perpendicular fashion is greater and that result in higher values of FQY. It is worthwhile to note here that, as the concentration of NPs increases, the difference in FQY for spherical and star shaped NPs decreases indicating the increased population of perpendicularly aligned dipoles.

Conclusions

In conclusion, we have demonstrated that shape and concentration of the green synthesized gold nanoparticles alter the fluorescence as well as non-radiative energy transfer of fluorescein dye. In a hybrid mixture of gold nanoparticles-fluorescein mixture, even when the average nanoparticles size is same, the shape of the nanoparticles plays a crucial role in the non-radiative energy transfer mechanism, as manifested in the energy transfer efficiency evaluated using steady state fluorescence signal and thermal lens studies. In addition, for a given concentration of nanoparticles in the mixture, the anisotropy in plasmonic field makes star shaped particles as an optical ruler that can probe larger distances as compared to spherical gold nanoparticles. The difference in probing distance becomes larger as the concentration of nanoparticles increases in the mixture. Moreover, the spherical gold nanoparticles for which dipoles are parallel to the surface act as more efficient quencher for fluorescein dye as compared to star shaped nanoparticles, evidenced by the corresponding fluorescence quantum yield values. These studies clearly show that, by tailoring shape and concentration of green synthesized nanoparticles, it is possible to control the optical properties of fluorescein dye in a simple dye-NP mixture. Such systems have potential applications in chemical and biological sensing, microscopy, catalysis and solar cells.

Acknowledgements

Authors gratefully acknowledge financial support from KSCSTE (Kerala State Council for Science, Technology and Environment), Trivandrum, India, through the project F.No.002/SRSPS/2007/CSTE. AK also acknowledges the support given by UGC, India.

References

1. H. Tao, X. Liao, M. Xu, X. Xie, F. Zhong and Z. Yi, Anal. *Methods*, 2014, **6**, 2560-2565.

2. C. S. Yun, A. Javier, T. Jennings, M. Fisher, S. Hira, S. Peterson, B. Hopkins, N.O. Reich and G. F. Strouse, *J. Am. Chem. Soc*., 2005, **127**, 3115-3119.

3. S. T. Kochuveedu, and D. Ha Kim, *Nanoscale*, 2014, **6**, 4966-4984.

4. S. Raut, R. Rich, P. Fudala, S. Butler, R. Kokate, Z. Gryczynski, R. Luchowski and I. Gryczynski, *Nanoscales*, 2014, **6**, 385-391.

5. D. Cheng and Q-H. Xu, *Chem. Comm.,* 2007, 248-250.

6. C. Xue, Y. Xue, L. Dai, A. Urbas and Q. Li, *Adv. Opt. Mat*., 2013, **1**, 581-587.

7. C. J. Breshike, R. A. Riskowski, and G. F. Strouse, *J. Phys. Chem. C*, 2013, **117**, 23942-23949.

8. S. Saraswat, A. Desireddy, D. Zheng, L. Guo, H. P. Lu, T. P. Bigioni and D. Isailovic, *J. Phys. Chem. C*, 2011, **115**, 17587-17593.

9. B. R. Kumar, N. S. Basheer, A. Kurian and S. D. George, *Int. J. Thermophys*., 2013, **34**, 1982-1992.

10. S. Mayilo, M. A. Kloster, M . Wunderlich, A. Lutich, T. A. Klar, A. Nichtl, K. Kürzinger, F. D. Stefani, and J. Feldmann, *Nanoletters*, 2009, **9**, 4558-4563.

11. R. Schreiber, J. Do, E-M. Roller, T. Zhang, V. J. Schüller, P. C. Nickels, J. Feldmann, and T. Liedl, *Nat. Nanotechnol*., 2014, **9**, 74-78.

12. K. Saha, S. S. Agasti, C. Kim, X. Li and V. M. Rotello, *Chem. Rev*., 2012, **112**, 2739–2779.

13. E. C. Dreaden, A. M. Alkilany, X. Huang, C. J. Murphy and M. A. El-Sayed, *Chem. Soc. Rev*., 2012, **41**, 2740-2779.

14. M. Stratakis and H. Gracia, *Chem. Rev*., 2012, **112**, 4469-4506.

15. S. Iravani, *Green Chem*,, 2011, **13**, 2638-2650.

16. S. He, Z. Guo, Y.Zhang, S. Zhang, J. Wang, and N. Gu, *Mater. Lett*., 2007, **61**, 3984-3987.

17. P. Mukherjee, A. Ahmad, D. Manda, S. Senapati, S. R. Sainkar, M. I. Khan, R. Ramani, R. Parischa, P. V. Ajayakumar, M. Alam, M. Sastry and R. Kumar, *Angew. Chem. Int. Ed*., 2001, **40**, 3585-3588.

18. O. V. Kharissova, H. V. R. Dias, B. I. Kharisov, B. O. Perez and V. M. J. Perez, *Trends in Biotechnol*., 2013, **31**, 240-248.

19. M. Fischer and J. Georges, *Chem. Phys. Lett*., 1996, **260**, 115-118.

20. C.V. Bindhu, S.S. Harilal, G. K. Varier, R. C. Issac, V. P. N. Nampoori and C. P. G. Vallabhan, *J. Phys. D. Appl. Phys*., 1996, **29**, 1074-1079.

21. S. Link and M. A. El-Sayed, Int. Rev. Phys. Chem., 2000, **19**, 409-453.

22. C. L. Nehl and J. H. Hafner, *J. Mater. Chem*., 2008, **18**, 2415-2419.

23. C. L. Nehl, H. Liao and J. H. Hafner, *Nanolett*., 2006, **6**, 683-688.

24. D.Margulies, G. Melman and A. Shanzer, *Nat. Mater*., 2005**, 4**, 768-771.

25. D. M. Togashi, B. Szczupak, A. G. Ryder and A. Calvet, *J. Phys. Chem*. *A*, 2009, **113**, 2757-2767.

26. X. Liu, M. Atwater, J. Wang, Q. Hou, *Colloids Surfaces B: Biointerfaces* , 2007, **58,** 3–7.

27. R. Sjoback, J. Nygren, M. Kubista, *Spectrochim. Acta part A,* 1995, **51**, L7-L21.

28. A. Kurian, S.D. George, C. V. Bindhu, V. P. N. Nampoori and C. P. G. Vallabhan, *Spectrochim. Acta Mol. Biomol. Spectros.,* 2007**, 67**, 678-682.

29. A. Kurian, K. P. Unnikrishnan, S.D. George, P. Gopinanth, V. P. N. Nampoori and C. P. G. Vallabhan, *Spectrochim. Acta Mol. Biomol. Spectros.,* 2003, **59,** 487-491.

30. N. S. Basheer, B. R. Kumar, A. Kurian and S.D. George, *Appl. Phys. B*, 2013, **113**, 581-587.

31. C. Fan, S. Wang, J. W. Hong, G. C. Bazan, K. W. Plaxco, and A. J. Heeger, *Proc. Natl.Acad. Sci,* 2003, **100,** 6297-6301.

32. B. I. Ipe, K. G. Thomas, S. Barazzouk, S. Hotchandani and P. V. Kamat, *J. Phys. Chem. B*, 2002, **106**, 18-21.

33. T. Sen, K. K. Haldar and A. Patra, *J. Phys. Chem. C*, 2008, **112**, 17945-17951.

34. K. K. Haldar, T. Sen and A. Patra, *J. Phys. Chem. C,* 2008, **112**, 11650-11656.

35. B. Valeur, Wiley-VCH, Weinheim, 2002.

36. J. R. Lakowicz, Plenum Press, New York, 1986.

37. M. Inokutti and F. Hiryama, *J. Chem. Phys*., 1965, **43,** 1978-1989.

38. B. N. J. Persson and N. D. Lang, *Phys.Rev.B,* 1982, **26**, 5409 -5415.

39. F. Stefani, K. Vasilev, N. Bocchio, N. Stoyanova, and M. Kreiter, *Phys. Rev. Lett.*, 2005, **94**, 023005-1-4.

40. E. Dulkeith, A. C. Morteani, T. Niedereichholz, T. A. Klar, J. Feldmann, S. A. Levi, F. C. J. M van Veegel, D. N. Reinhoudt, M. Möller and D. I. Gittins, *Phys. Rev. Lett.*, 2002**, 89**, 203002-1-4.

41. N.S. Basheer, B.R. Kumar, A. Kurian and S.D. George, *J. Lum*., 2013, **137**, 225-229.

42. F. Hao, C. L. Nehl, J. H. Hafner and P. Nordlander, *Nano Lett*., 2007, 7, 729-732.

43. M. Sukharev, N. Freifeld, A. Nitzan, *J. Phys. Chem. C*, 2014, 118, 10545-10551.

44. S. Halivni, A. Sitt, I. Hadar, and U. Banin, *ACS Nano*, 2012, **6**, 2758-2765.

45. A. Santhi, U. L. Kala, R. J. Nedumpara, A. Kuiran, M. R. P. Kurup, P. Radhakrishnan and V. P. N. Nampoori, *Appl. Phys. B,* 2004, **79**, 629-633.

46. C. E. Lopez, T. Dominguez and R. E. de Araujo, *Opt. Express*, 2013, **21**, 18592-18601.

Table 1. Energy transfer efficiency and dye-NPs distance for differently shaped NPs.

Concentration of gold nanofluid (nM)	Energy transfer efficiency (%)				Distance (Å)			
	Star shaped AuNPs		Spherical shaped AuNPs		Star shaped AuNPs		Spherical shaped AuNPs	
	Thermal lens method	Fluorescence method	Thermal lens method	Fluorescence method	Thermal lens method	Fluorescence method	Thermal lens method	Fluorescence method
0.13	14.42	14.59	19.62	20.04	111.44	111.06	101.58	100.91
0.51	22.13	25.44	30.70	31.25	95.79	93.42	87.51	86.95
1.79	42.83	41.83	61.85	60.73	76.74	77.53	63.27	64.02
2.57	51.60	50.09	70.93	68.82	70.26	71.33	57.12	58.57

Figure Captions

Figure 1. TEM image of AuNPs prepared using a) piper nigrum (b) cinnamomum verum as reducing agents. The inset shown the TEM image of a single AuNP

Figure 2. Absorption spectrum of a) star shaped AuNPs and b) spherical AuNPs.

Figure 3. Absorption spectrum of a) fluorescein and b) fluorescein-star shaped AuNPs c) fluorescein-spherical AuNPs.

Figure 4. Fluorescence of a) fluorescein (2.4x10-4 M) and fluorescein-star shaped AuNPs mixtures with b) 0.13 nM c) 0.51 nM d) 1.79 nM e) 2.57 nM AuNPs.

Figure 5. Fluorescence of a) fluorescein (2.4x10-4 M) and fluorescein-spherical shaped AuNPs mixtures with b) 0.13 nM c) 0.51 nM d) 1.79 nM e) 2.57 nM AuNPs.

Figure 6. Absorption spectrum of a) spherical NPs b) star shaped NPs and emission spectrum of c) fluorescein d) fluorescein-star shaped AuNPs e) fluorescein-spherical AuNPs.

Figure 7. Stern –Volmer plot for spherical AuNPs-fluorescein mixture a) fluorescence method b) thermal lens method.

Figure 8. Stern–Volmer plot of star shaped AuNPs-fluorescein mixture a) fluorescence method b) thermal lens method.

Figure 9. Fluorescence Quantum Yield of a) star shaped and b) spherical shaped AuNPs- fluorescein mixture.

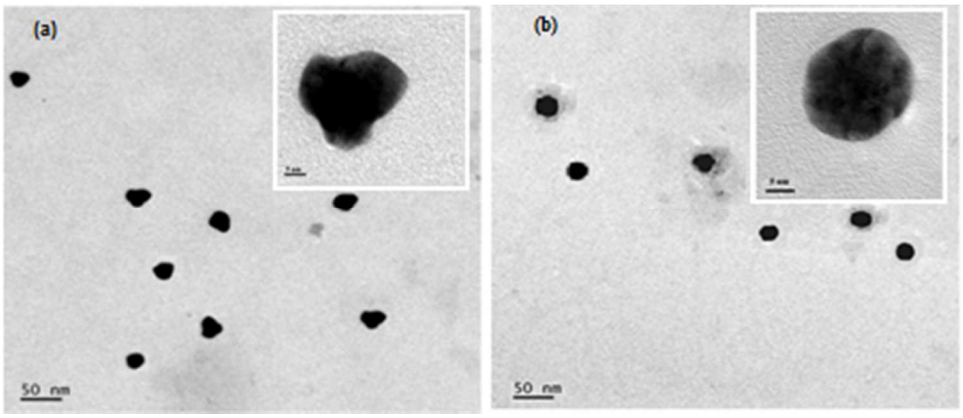

Figure 1. TEM image of AuNPs prepared using a) piper nigrum (b) cinnamomum verum as reducing agents. The inset show TEM image of a single AuNP

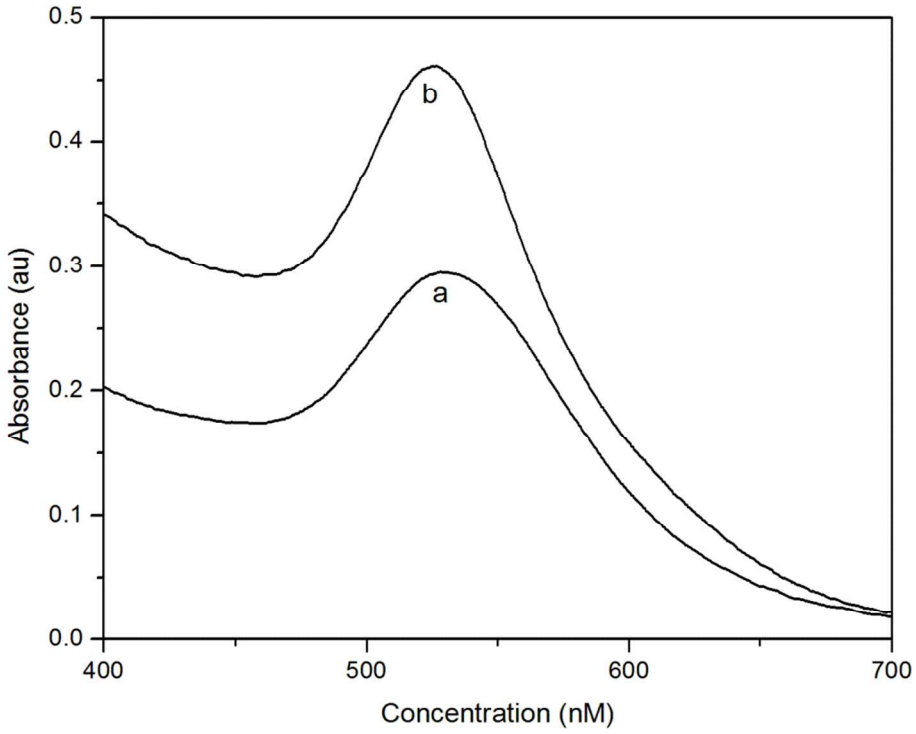

Figure 2. Absorption spectrum of a) star shaped AuNPs and b) spherical AuNPs.

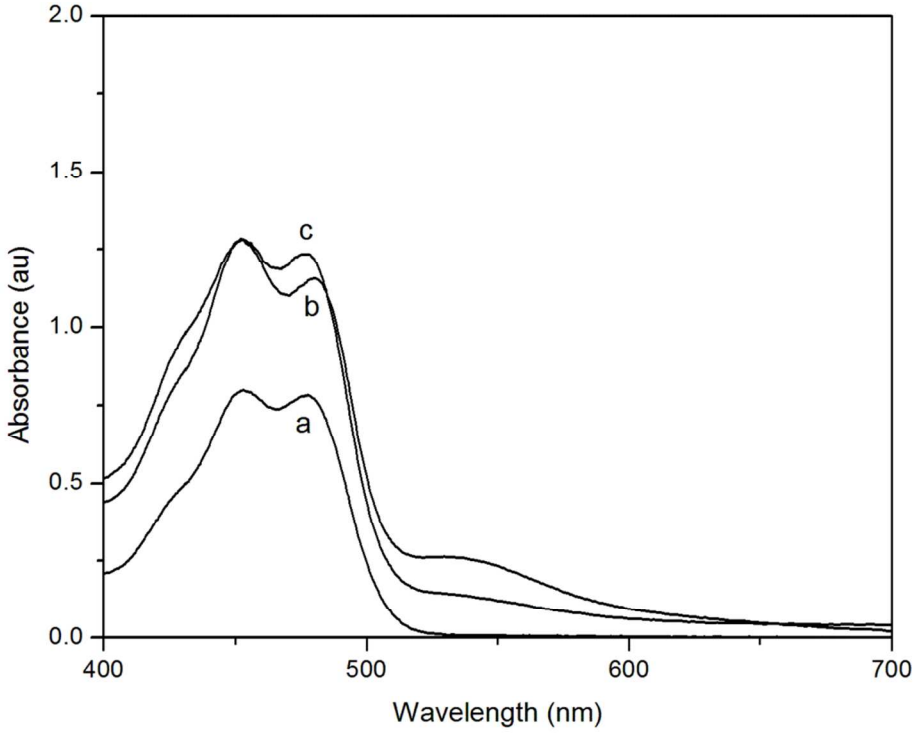

Figure 3. Absorption spectrum of a) fluorescein and b) fluorescein-star shaped AuNPs c) fluorescein-spherical AuNPs.

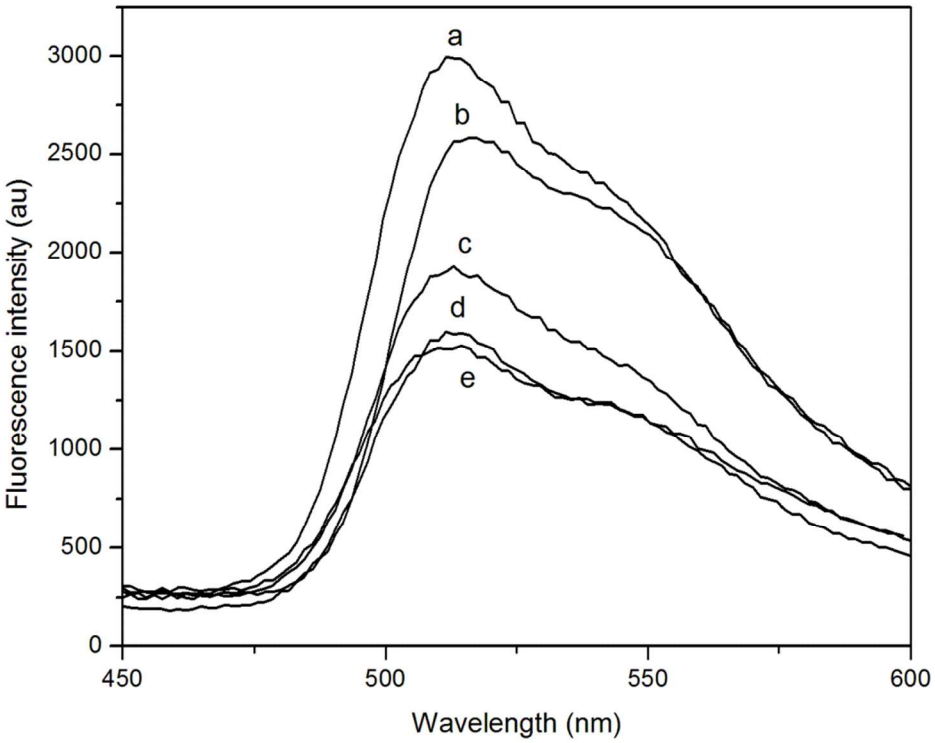

Figure 4. Fluorescence of a) fluorescein (2.4x10-4 M) and fluorescein-star shaped AuNPs mixtures with b) 0.13 nM c) 0.51 nM d) 1.79 nM e) 2.57 nM AuNPs.

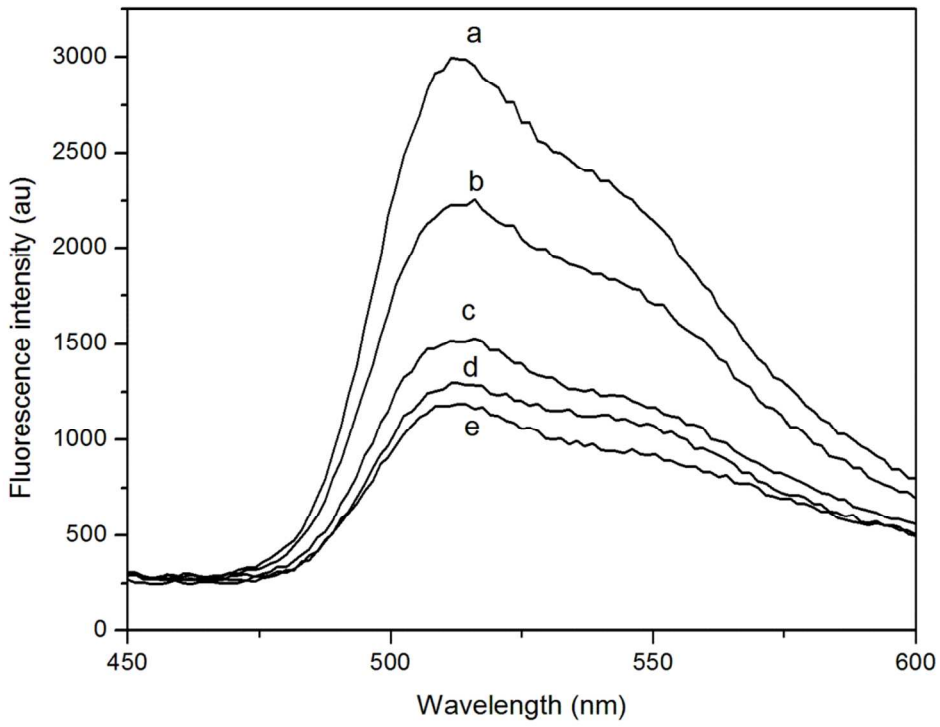

Figure 5. Fluorescence of a) fluorescein (2.4x10-4 M) and fluorescein-spherical shaped AuNPs mixtures with b) 0.13 nM c) 0.51 nM d) 1.79 nM e) 2.57 nM AuNPs.

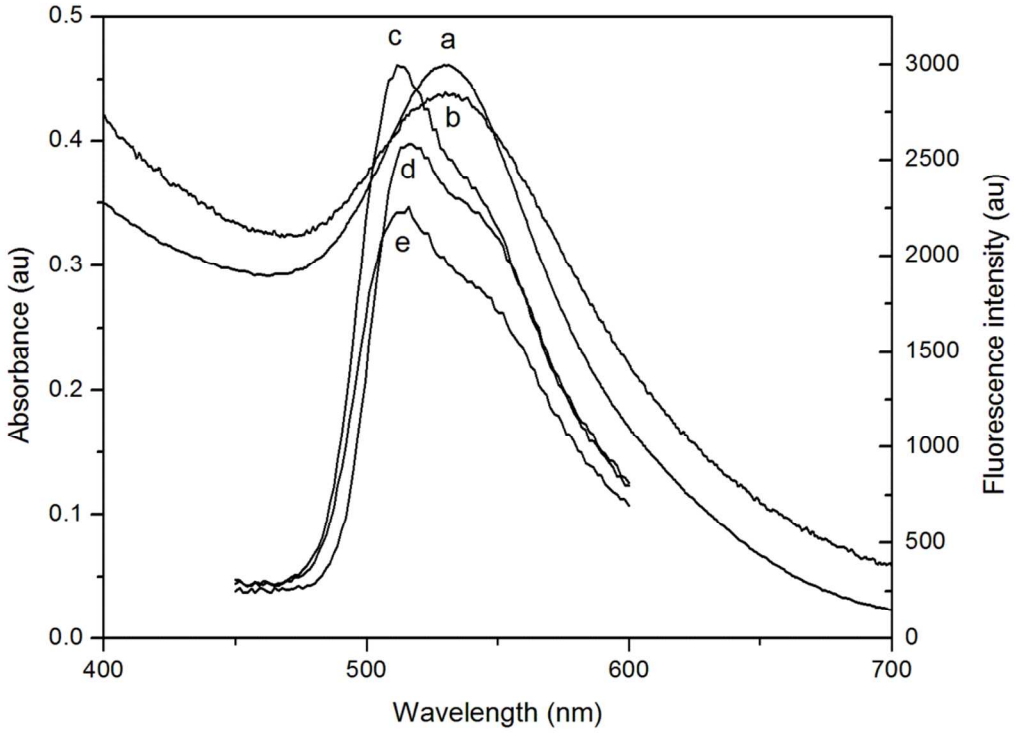

Figure 6. Absorption spectrum of a) spherical NPs b) star shaped NPs and emission spectrum of c) fluorescein d) fluorescein-star shaped AuNPs e) fluorescein-spherical AuNPs.

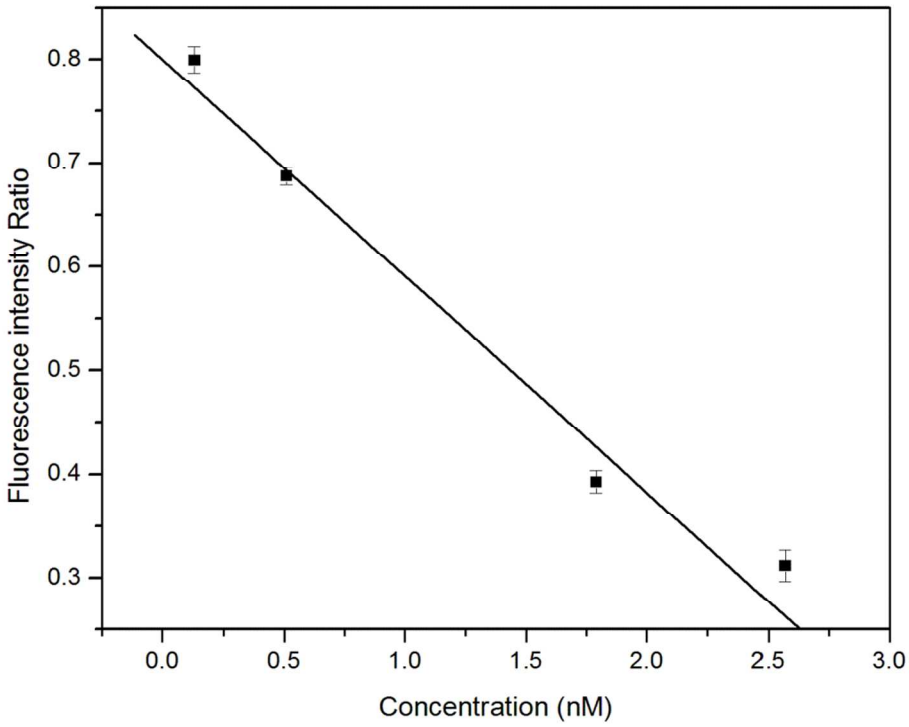

(a)

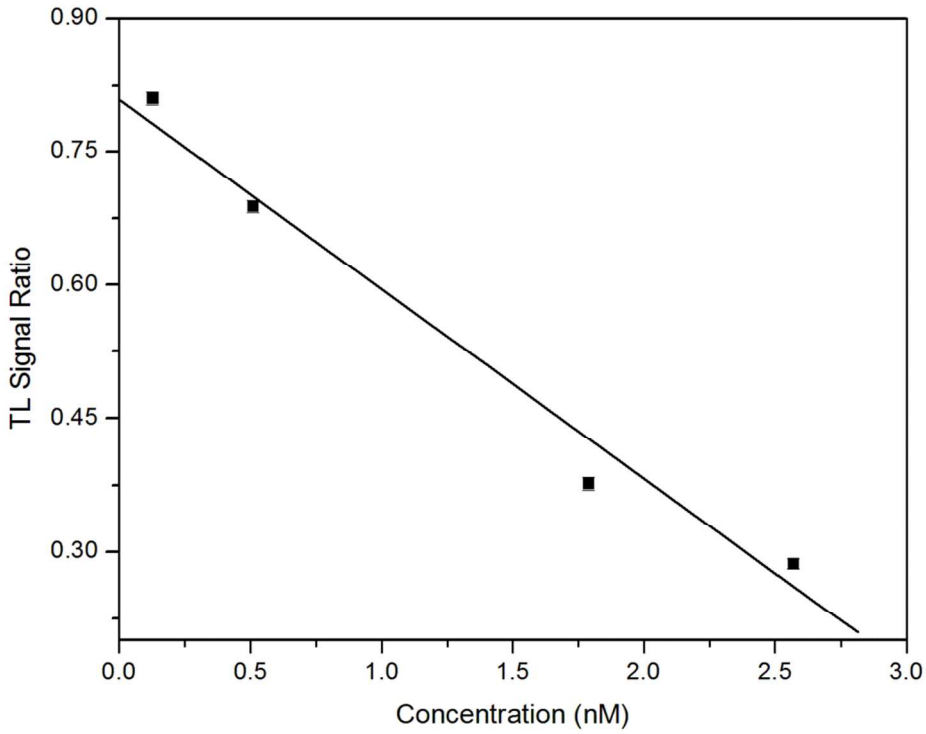

(b)

Figure 7. Stern –Volmer plot for spherical AuNPs-fluorescein mixture a) fluorescence method b) thermal lens method.

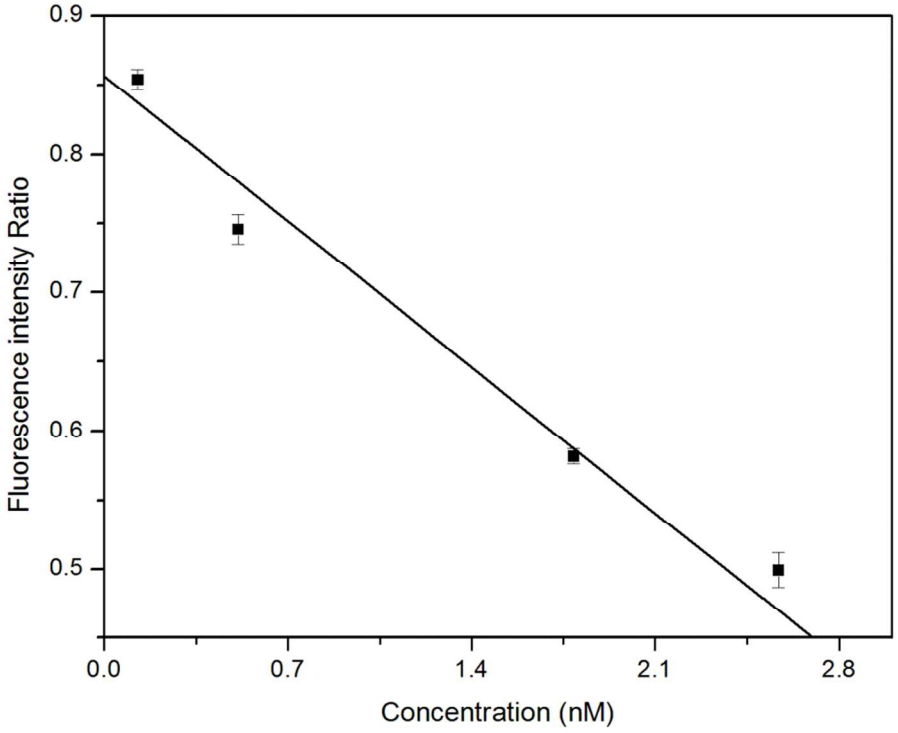

(a)

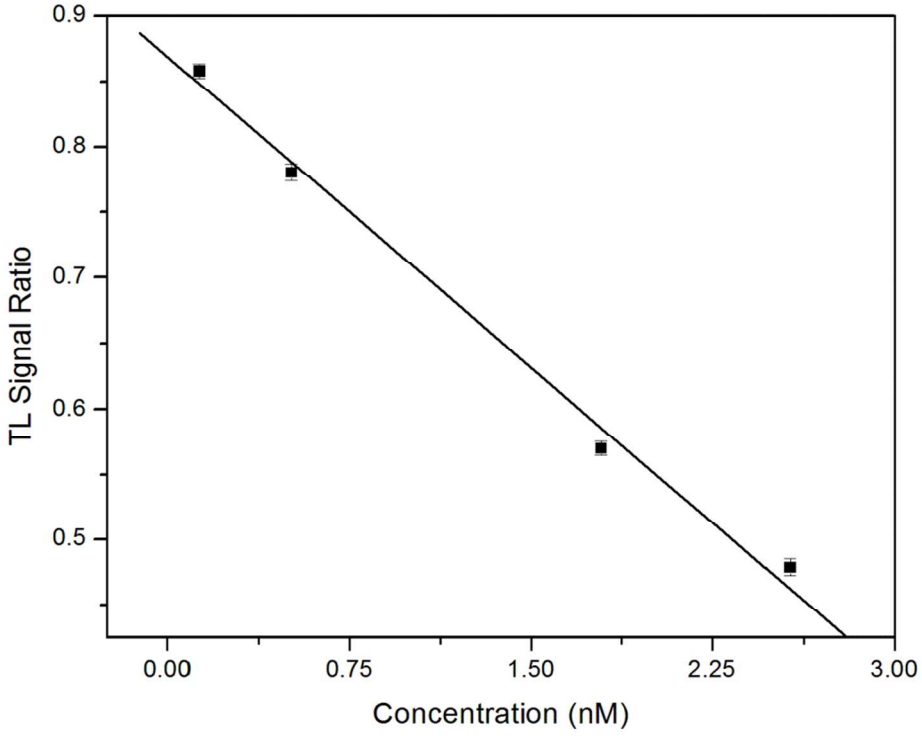

(b)

Figure 8. Stern–Volmer plot of star shaped AuNPs-fluorescein mixture a) fluorescence method b) thermal lens method.

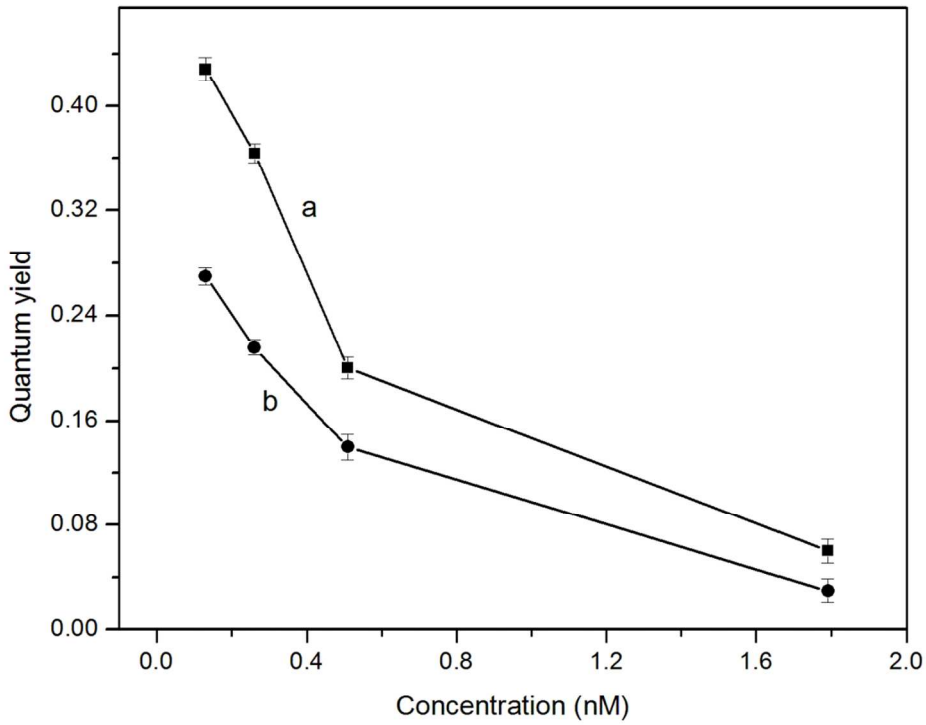

Figure 9. Fluorescence Quantum Yield of a) star shaped and b) spherical shaped AuNPs- fluorescein mixture.